Supplementary materials and methods

Cell lines

KRAS-mutant iCCA cell lines, HuCCT1 (*KRAS*^{G12D}) and RBE (*KRAS*$^{G12V)}$) and *KRAS*-wildtype CCA cell lines HuH28 and WITT were obtained from JCRB Cell Bank or kindly provided by Gregory Gores (Mayo Clinic, Rochester, USA). Primary iCCA cell lines (*KRAS*-mutant cell line CCC16 (*KRAS*^{G12D}) and *KRAS*-wildtype cell line CCC33) were established at the University Medical Center, Mainz in accordance with ethical guidelines [1]. Primary mouse Parp1$^{-/-}$ (Kras/Tp53 Parp1$^{-/-}$) cell line was established at the University Medical Center Mainz upon extraction of the tumors from the HDTV mouse model. *Kras*^{G12D}*;Rb*^{del}*;Tp53*^{del} cell line was kindly provided by Ursula Ehmer. None of the cell lines harbor a loss of function variant in *BRCA1/2* [1–4]. HuCCT1, RBE, WITT, CCC16, CCC33, *Kras*^{G12D}*;Rb*^{del}*;Tp53*^{del}, were cultivated in DMEM (Gibco), supplemented with 1 unit/ml penicillin/streptomycin (P/S, Sigma Aldrich), 5% FCS (Pan-Biotech). HuH28 cells were cultivated in RPMI-1640 medium (Sigma Aldrich) (1 unit/ml P/S, 5% FCS) (Pan-Biotech). All cell lines were maintained at 37°C and 5% CO_2, routinely mycoplasma tested and, when possible, either purchased fresh or authenticated by STR testing.

Nucleic acid extraction and RNA sequencing

DNA was extracted by performing peqGOLD Tissue DNA mini kit (VWR International) following the manufacturer's instructions. Total RNA was extracted using peqGOLD total RNA kit (VWR International) according to the manufacturer's instructions. RNA quality and purity was determined by Nanodrop ND-1000 spectrophotometer (NanoDrop Technologies) and the integrity was measured by Agilent 2100 Bioanalyzer (Agilent). RNA sequencing was performed using Illumina Novaseq 6000. DESeq2 pipeline was used for differential expression analysis. Principal Components Analysis (PCA) and unsupervised hierarchical clustering were conducted using ComplexHeatmap [5]. Ingenuity Pathway Analysis (IPA) online tool provided by Qiagen was used to identify the regulation of pathways and networks. The scoring system provided by IPA tool was employed to identify significantly regulated pathways [6]. Gene set enrichment analysis (GSEA) was performed using GSEA software provided by Broad Institute (Broad Institute Inc, Cambridge, USA). Gene sets with nominal $p<0.05$ and false discovery rate (FDR)<0.25 were considered enriched in a priori defined sets of genes [7]. Gene expression profiling interactive analysis (GEPIA2) was employed for gene expression and correlation analyses of data sets of cholangiocarcinoma (CHOL) and liver hepatocellular carcinoma (LIHC) from The Cancer Genome Atlas Program (TCGA). Differential analysis was calculated with one-way ANOVA, using disease state (tumor or normal) after log2(TPM+1) transformation [8].

Quantitative real-time polymerase chain reaction

Two-step reverse-transcription quantitative polymerase chain reaction using iScript cDNA Synthesis kit (Bio-Rad Laboratories), SYBR Green Master-Mix (Bio-Rad Laboratories) and CFX Connect (Bio-Rad Laboratories) was performed. Oligonucleotide primers were designed using Primer3 v.0.4.0 (http://frodo.wi.mit.edu/primer3/) as described before (*PARP-1* forward 5‘-CGAATGCCAGCGTTACAAGC-3‘, *PARP-1* reverse 5‘-AACATGTAGCCTGTCACGGG-3‘, *PARP-2* forward 5‘-TCCCCTGCCAAGAAAACTCG-3‘, *PARP-2* reverse 5‘-TCAGAGACCCTTTTGCTGGC-3‘, *GAPDH* forward 5’-CAACGACCACTTTGTCAAGC-3’, *GAPDH* reverse 5’-TCTTCCTCTTGTGCTCTTGC-3’, *CHK1* forward 5’-GGCTTGGCAACAGTA-3’ *CHK1* reverse 5’- CAGGACCAAACATCA-3’, *RAD51* forward 5’-GCAGTGGCTGAGAGGTATGGT-3’ *RAD51* reverse 5’-TTCTGTAAAGGGCGGTGGCA-3’, *XRCC2* forward 5’-ACCTTCTCATGCCTCTCGACG-3’ *RAD51* reverse 5’-TGCTTCACCAGTTGCTGCCA-3’, *CDC25C* forward 5’-TGGCCAAGGAAAGCTCAGGA-3’ *CDC25C* reverse 5’-TTGGCAGCGCACATACCTTG-3’) (Eurofins).

Western blotting

Cell lysates were prepared using M-PER tissue extraction buffer (Thermo Fisher) containing complete protease inhibitor cocktail (Gibco). 25 µg of protein lysate were separated by SDS-PAGE and transferred onto nitrocellulose membrane (Sigma Aldrich). Membranes were probed with the indicated antibodies (beta-Actin Clone 2Q1055 (mouse, monoclonal, Santa Cruz #sc-58673); PARP-1 (46D11) (rabbit, monoclonal, Cell signaling #9532), PARP-2 (rabbit, monoclonal, EMD Millipore #MABE18), CHK1 (mouse, monoclonal, Santa Cruz #SC8408)). Quantification of expression levels was performed by densitometric analyses using ImageJ (NIH).

siRNA-mediated knockdown

For transfection, cells were seeded at low confluency (30-50%) in 6-well plates. After 24 h 100 pmol siRNA (non-sense control, two different siRNAs targeting *PARP-1,* Eurofins) was introduced by using transfection reagent Lipofectamine 3000 (Thermo Fisher) following the manufacturer’s instructions. Subsequent functional assays were conducted 72 h after transfection.

CRISPR/Cas9-mediated knockout

Cells transfected with Clustered Regularly Interspaced Short Palindromic Repeats/Caspase9 (CRISPR/Cas9) plasmids (pNV-sgRNA-Cas9-2A-GFP; abm; 2 µg) were transferred to 10 cm dishes and after reaching 80-90% confluency sorted into single cells based on the integrated selection marker GFP using BD FACSAria optimally 5-7 days after transfection (Core Facility

Flow Cytometry, Paul-Klein Center for Immune Intervention, University Medical Center Mainz). Successful knockout of single cell clones was verified by Western blot analysis and Sanger Sequencing (StarSEQ GmbH).

Dose response and viability assay

Cell viability was determined using a colorimetric assay (WST-1) following the manufacturer's protocol (Roche). Inhibitor stock solutions were prepared by dissolving in dimethyl sulfoxide (DMSO; Carl Roth), according to the manufacturer's recommendations. Working solutions were prepared by dilution in DMEM (10% FCS, 1% P/S). Into each 96-well, $5x10^3$ cells were plated for 24 h before treatment followed by administration and incubation with inhibitors for 72 h. Olaparib (Chemietek) was applied in the range of concentrations from 8-2048 µM alone or in combination with Doxorubin (60 nM) (Sellekchem), while Rabusertib (TargetMol) was applied from 0.25-40 µM alone in combination with Olaparib. Cisplatin was applied in the range from 1.25-80 µM and Gemcitabine from 0.325-20 µM together with Olaparib. KU57788 was applied in the range from 2.5-160 µM. Cell viability was expressed as the absorbance in the treatment group compared to control group as viability percent ± SD (n=3). Median inhibitory concentration (IC50) values were calculated from dose-response curves of three independent experiments by nonlinear regression using Prism software (GraphPad Software). Synergistic effects were determined using SynergyFinder online tool (http://www.synergyfinderplus.org/#!/)

Colony and sphere formation assay

Cells were treated for 72 h with the cell line specific IC50 of Olaparib, or siRNA-mediated knockdown of *PARP-1*. $1x10^3$ cells were plated on 6-well plates for colony formation (CFU) and $1x10^3$ cells were plated on 48-well plates for sphere formation (SFU) assay into a semi-solid soft agar (Carl Roth). After 14 days colony and sphere formation capacities were determined and represented as number of colonies/spheres for each treatment group in comparison to the control group in percentage.

Cell cycle analysis

Cells were treated with IC25 concentration of Olaparib for 48 hours, harvested and cell cycle analysis was performed using flow cytometry and propidium iodide staining protocol. A total of 100000 events were recorded and different phases of the cell cycle were determined using FlowJo V10.

Detection of oxidative stress

2',7'-dichlorodihydrofluorescein-diacetate (DCH2FC-DA; Sigma Aldrich) was used to monitor oxidative stress in the iCCA cells. The method is based on the intake of non-fluorescent DCH2FC-DA into the cells by diffusion, where it gets hydrolyzed to 2',7'-dichlorofluorescin (DCFH) and is trapped inside the cells. Upon cellular oxidative stress, DCFH is oxidized by ROS to the highly fluorescent form 2',7'-dichlorofluorescein (DCF), which was detected at a specific excitation/emission spectrum (495 nm / 535 nm) using a microplate spectrofluorometer (TECAN infinite M 200Pro). Oxidation of DCFH was correlated quantitatively to the level of oxidative stress mediated by H_2O_2 (Carl Roth) and other reactive oxygen species.

Induction of DNA damage via irradiation

The iCCA cell lines were seeded on coverslips placed in 3 cm plates ($1x10^5$ cells) and cultured in DMEM (10% FBS) for 24 hours. Next, cells were placed into an irradiator (Gammacell 2000) and irradiated with 5 Gy (500 rad = 1:59 sec). After incubation for 1 hour at 37°C, cells were fixed, and immunofluorescence staining was performed. Cells were stained for phospho-γH2AX (Cell Signaling Technology, 1:500) using standard protocol and visualized and recorded using a Laser Scanning Microscope LSM-710 (Zeiss) with 63 x magnification oil objective.

Experiments involving animals

All procedures were performed in accordance with the National Animal Protection Guidelines following approval by the local authorities. The origin and properties of the mouse strain with *Parp-1* knockout (129/Sv x C56BL/6J genetic background) was previously described [9,10]. Plasmids for HDTV were kindly provided by Matthias S. Matter, Institute of Pathology, University Hospital Basel, Switzerland. HDTV with plasmid solutions of pT3-EF1a-$Kras^{G12V}$/pT3-EF1a-shRp53-844-866 *or* pT3-EF1a-myrAkt/pT3-EF1a-Nicd (myc-tagged) in combination with pCMV-HSB2 plasmid (ratio 1:5) was performed as described before [11–13]. Experimental design comprised three experimental groups with 7-8 week old male *Parp-1*$^{+/+}$ and *Parp-1*$^{-/-}$ mice (genotype was determined beforehand). Animals were monitored weekly for signs of liver failure due to tumor growth and significant changes in body weight. Mice injected with *Kras/Tp53* were sacrificed after 10 weeks, mice injected with *Akt/Nicd* after 7-8 weeks. Quantification was performed by liver weight / body weight ratio and a scoring system to assess the morphological differences. After sacrifice, the liver was dissected and either fixed in 4% PFA or preserved at -80°C.

Immunohistochemistry and confocal microscopy

Tissue samples were fixed in 4% PFA, embedded in paraffin and cut into 3.5 µm sections. H&E staining was performed by standard techniques using Mayer's Hemalaun (Merck KGaA) and Eosin-y Alcoholic solution (Thermo Fisher). Immunohistochemistry was done by automated immunostaining with DAB staining (Dako) according to the manufacturer's instructions. Visualization was performed by a Zeiss Axioskop microscope with 5x and 10x magnification objectives and analyzed in AxioVision 3.1 software.

Tissue microarray was performed as follows: paraffin-embedded formalin-fixed (FFPE) tissue samples from 197 patients with Cholangiocarcinoma diagnosed with Cholangiocarcinoma at the Institute of Pathology, University Medical Center Mainz, between 2006 and 2020 were collected. These samples were processed following the Tissue Biobank's protocols at the University Medical Center Mainz. Tissue microarrays (TMAs) featuring 2 mm cores were assembled. Immunohistochemistry (IHC) analysis was conducted on FFPE specimens sliced to a thickness of 2-4 µm. A rabbit monoclonal antibody targeting PARP-1 (clone 46D11; Cell Signaling Technology Europe B.V., Leiden, Netherlands) was employed at a 1:600 dilution. The immune reactive score (IRS) system was utilized to assess PARP-1 immunohistochemistry [14], generating scores ranging from 0 to 12, derived from multiplying the proportion of positive cells (scored 0–4) by the staining intensity (scored 0–3). The mean IRS was determined for patients with the same entity.

RPPA

Functional Proteomics RPPA Core facility, supported by MD Anderson Cancer Centre, Houston, Texas. Proteins were extracted from the cell pellets, denatured using 1% SDS + B-Me, serial diluted and arrayed on nitrocellulose-coated slides and the antigen-antibody reaction was determined. The emitted signals were captured by tyramide dye deposition and a DAB colorimetric reaction. The stained slides were scanned on a Huron TissueScope scanner to produce a 16-bit till image and sample densities were quantified by Array-Pro Analyser. Obtained data obtained was further quantitatively analyzed using Supercurve software and presented as expression relative to standard control cells on the array.

STRING

Explore functional connections with the biological implications between targets of interest (i.e., CHK1, PARP1 RAD51, CDC25C, XRCC2) the STRING database (https://string-db.org/) (version 12.0) was used. Computational prediction of direct/indirect protein-protein association is based on already reported findings from other databases [15].

Statistical analyses

Statistical analyses were performed using Student's t-test, one-way ANOVA, or Mann-Whitney U test as indicated. $p \leq 0.05$ were considered statistically significant. All results were presented as means ± standard deviation (SD) from at least three independent experiments.

Supplementary figures

Figure S1: Transcriptomic, correlation and survival analysis of *PARP-1* and *KRAS* expression in TCGA and own dataset.

A) *PARP-1* and B) *KRAS* gene expression profiles (TCGA) in cholangiocarcinoma vs. normal liver tissue (CHOL) and liver hepatocellular carcinoma vs. normal liver tissue (LIHC) presented in box plots. Values of p<0.01 (*) were considered as of significant difference. red=tumor, blue=liver C) Multiple comparisons of *PARP-1* and *KRAS* expression in cholangiocarcinoma vs. normal liver tissue (CHOL) and hepatocellular carcinoma vs. normal liver tissue (LIHC) (log2(TPM+1) D) Pair-wise gene expression correlation analysis of *PARP-1* and *KRAS* expression in cholangiocarcinoma (CHOL) (Pearson correlation coefficient, TCGA CHOL Tumor/TCGA CHOL normal). E) Pair-wise gene expression correlation analysis of *PARP-1* and *KRAS* expression in hepatocellular carcinoma (LIHC) (Pearson correlation coefficient R, TCGA LIHC Tumor/TCGA LIHC normal). F) Immunohistochemical analysis of PARP1 expression in a human cohort of 194 iCCA patients. PARP-1 was evaluated using the mean immunoreactive score (IRS), which ranges from 0 to 12. A score of 0 indicates no staining, whereas a score of 12 signifies the strongest staining possible p<0.0001 (***). G) Expression level of *PARP1* in the Andersen iCCA cohort in comparison with the surrounding liver and normal bile ducts H) Chiang's liver cancer proliferation signature shows a positive correlation with *PARP1* expression. I) Estimated median overall survival and recurrence free survival for iCCA patients with and without *KRAS* mutation obtained from cBioportal. Shown is Kaplan-Meir curve with a total of 412 patients.

Figure S2: Effect of PARP-1 inhibition via Olaparib treatment on cell viability, colony and sphere formation capacity and synergistic effects with approved iCCA drugs.

A) Shown are dose-response curves of *KRAS*-mutant and *KRAS*-wildtype iCCA cell lines treated with increasing concentrations of Olaparib to determine IC50 value and impact on proliferation. Mean ± SD, n=3, p<0.05 (*), p<0.01 (**). B) Phases of cell cycle after 48 h treatment with IC25 concentration of Olaparib. Shown are normalized values to untreated control cells. Mean ± SD, n=3, p<0.01 (**). C) Colony and sphere formation assay shown as % of control after Olaparib treatment in *KRAS*-mutant and *KRAS*-wildtype iCCA cell lines. Mean ± SD, n=3, p<0.05 (*), p<0.001 (***). D) Synergistic effects of Olaparib/Cisplatin and Olaparib/Gemcitabine in *KRAS*-mutant and *KRAS*-wildtype iCCA cell lines. Plots indicate level of synergism between investigated drugs, where red color represents synergism and green color antagonism. Bars on the right represent quantification of an average synergy score between *KRAS*-mutant and *KRAS*-wildtype iCCA cell lines. Mean ± SD, n=3, p<0.001 (***). E) Shown are IC50 values for primary CCC33 and CCC16 cell lines after treatment with KU-5778 inhibitor. Mean ± SD, n=3.

Figure S3: PARP-1 protein expression in primary and established iCCA cell lines after CRISPR/Cas9-mediated knockout.

A) Representative Western blot of PARP-1, PARP-2, and β-actin protein levels after *PARP-1* KO in *KRAS*-mutant (HuCCT1, RBE; red) and *KRAS*-wildtype iCCA cell lines (CCC33, WITT; blue).

Figure S4: Enriched gene sets in *KRAS*-mutant iCCA cell lines upon *PARP-1* KO.

A) Clinical endpoints and networks significantly regulated in *KRAS*-mutant iCCA cell lines upon *PARP-1* KO vs. control identified by IPA. The dashed line indicates the significance threshold of –log(p-value>1.3). Shown are z-scores of respective canonical pathways (positive z-score =red/activated, negative z-score = blue/inhibited). B) Gene set enrichment analysis (GSEA) in

KRAS-mutant iCCA cell lines upon *PARP-1* KO vs. control clones. The selection of gene sets was based on statistical significance calculated by nominal p<0.05 and FDR<0.25. NES indicates the degree of overexpression for each group at the peak of the entire gene set.

Figure S5: Regulatory mechanism of PARP1 in KRAS mutated human tissue and cell lines

A) Immunofluorescence staining of p-γH2AX foci by confocal microscopy. Shown is quantification of p-γH2AX foci in KRAS-mutant (RBE; red) and KRAS-wildtype iCCA cell lines (CCC33; blue) and their respective PARP-1 KO clones under control conditions and after irradiation with 5 Gy. Quantification indicating fold change of the number of cells with foci > 5 as % of total cell number. Mean ± SD, n=3, p < 0.05 (*), p < 0.01 (**). B) Shown are basal and H_2O_2-induced (25 µM H_2O_2) changes in redox status using ROS-indicator CM-H2DCF-DA in KRAS-mutant (RBE; red) and KRAS-wildtype iCCA cell lines (CCC33; blue) and their respective PARP-1 KO clones. Shown is the mean fluorescence intensity. Mean ± SD, n=3, p < 0.05 (*), p < 0.01 (**), p < 0.001 (***). C) Analysis of 5 KRAS mutated tissue samples and matched non-tumoral liver tissue. Vulcano plots are depicted with the log(fold change) of each gene and the –log(p adjusted) was calculated by performing Wald test. Selected genes associated with HR, c-NHEJ, and alt-NHEJ are colored and gene names are displayed. D) Gene set enrichment analysis (GSEA) of KRAS-mutant tumor. The selection of gene sets was based on statistical significance calculated by nominal p-value < 0.05 and FDR < 0.25. NES indicates the degree of overexpression for each group at the peak of the entire gene set. E) Normalized protein level in primary cell lines with (CCC16) and without (CCC33) *KRAS* mutation detected by Reverse-phase protein array (RPPA). Mean ± SD, n=5, p<0.05 (*), p<0.01 (**), p<0.001 (***).

Figure S6: Single cell analysis of DNA damage repair pathways in iCCA patients with or without *KRAS* mutations tumor cells

Average expression of genes involved in DNA damage repair pathways of A) DNA repair_Hallmarks, B) BER_KEGG and C) NHEJ_KEGG in malignant and non-malignant cells from iCCA patients with or without *KRAS* mutations.

Figure S7: Experimental design of iCCA tumor initiation via HTDV in *Parp-1*$^{+/+}$ and *Parp-1*$^{-/-}$ mice.

A) 7-8-weeks old mice were injected with i) 2000 µg HSB2-plasmid (empty vector control; EV); ii) 5000 µg *Kras*^{G12V}-plasmid, 5000 µg *shRp53*-plasmid and 2000 µg *HSB2*-plasmid (*Kras/Tp53*); or iii) 2500 µg *myrAkt*-plasmid, 2500 µg myc-tagged *Nicd*-plasmid and 1000 µg *HSB2*-plasmid (*Akt/Nicd*) and sacrificed at the age of 14-18 weeks. B) List shows information (ID, gender, bodyweight, liver weight on the day of sacrifice) of *Parp-1*$^{+/+}$ and *Parp-1*$^{-/-}$ mice injected with empty vector and plasmid combinations *Kras/Tp53* and *Akt/Nicd.* *Mouse was excluded after analysis of transcriptomic data (outlier analysis).

Figure S8: Histopathological classification of *in vivo* tumors.

A) Scheme of histopathological assessment of tumor sections induced by HDTV (*Kras/Tp53*; *Akt/Nicd)* in *Parp-1*$^{-/-}$ and *Parp-1*$^{+/+}$ mice. B) Table shows information (grading, number of foci, size, hematogenous spread) of paraffin-embedded tumor sections.

Figure S9: Quantification of immunohistochemistry staining in liver sections after HDTV with *Kras/Tp53* and *Akt/Nicd*.

Quantification of selected immunohistochemical markers (Parp-1, Ki67, and yH2ax) in liver sections of mice injected with A) *Kras/Tp53* and B) *Akt/Nicd*. The number of stained nuclei was determined by ImageJ and adjusted to control staining. Mean ± SD, n=5, p<0.05 (*), p<0.01 (**), p<0.001 (***).

Figure S10: Expression of the genes and proteins associated with defined pathways after HDTV with *Kras/Tp53* in *Parp-1*$^{-/-}$ and *Parp-1*$^{+/+}$ mice.

Cluster analysis of samples from Parp-1$^{-/-}$ and Parp-1$^{+/+}$ animals with Kras/Tp53 mutations. Analysis was performed based on the Broad Institute gene sets regulating cell cycle, Hippo signaling, apoptosis, MAPK, TGF-β using r-log values. A) Heatmaps and cluster analyses of Kras/Tp53 Parp-1$^{-/-}$ vs Parp-1$^{-/-}$ empty vector B) Heatmaps and cluster analyses of Kras/Tp53 Parp-1$^{-/-}$ vs of Kras/Tp53 Parp-1$^{+/+}$ C) Immunohistochemistry staining of selected proteins (Cdc25a, Caspase 3, Yap, and Mapk p38) of *Parp-1*$^{-/-}$*Kras/Tp53* mouse in normal and tumor tissue. Representative images of normal liver and tumor tissue from animal model are shown. Scale bars indicate 200 µm (20x magnification).

Figure S11: Enriched gene sets in *Parp-1*$^{-/-}$ mice injected with *Kras/Tp53* vs. *Parp-1*$^{+/+}$ mice.

A) Gene set enrichment analysis (GSEA) of *Parp-1*$^{-/-}$ mice injected with *Kras/Tp53* vs. *Parp-1*$^{+/+}$ mice. Selection of gene sets was based on statistical significance calculated by nominal p<0.05 and FDR<0.25. NES indicates degree of overexpression for each group at the peak of the entire gene set.

Figure S12: Differential expressed genes after HDTV with *Akt/Nicd* in *Parp-1*$^{-/-}$ vs. *Parp-1*$^{+/+}$ mice.

A) Unsupervised cluster and PCA plot of significant genes (p<0.05) after HDTV with *Akt/Nicd* in *Parp-1*$^{-/-}$ vs. *Parp-1*$^{+/+}$ mice. B) Canonical pathways and clinical endpoints and networks significantly regulated in tumors induced with *Akt/Nicd* in *Parp-1*$^{-/-}$ vs. *Parp-1*$^{+/+}$ mice identified by IPA. Dashed line indicated significance threshold of –log(p-value > 1.3). Shown are z-scores of respective canonical pathways (positive z-score = red/activated, negative z-score = blue/inhibited).

Figure S13: Enriched gene sets in *Parp-1*$^{-/-}$ mice injected with *Akt/Nicd* vs. *Parp-1*$^{+/+}$ mice.

A) Gene set enrichment analysis (GSEA) of *Parp-1*$^{-/-}$ mice injected with *Akt/Nicd* vs. *Parp-1*$^{+/+}$ mice. Selection of gene sets was based on statistical significance calculated by nominal p<0.05 and FDR<0.25. NES indicates degree of overexpression for each group at the peak of the entire gene set.

Figure S14: Regulatory mechanism of CHK-1 and PARP-1 in KRAS mutated primary human cell lines

A) Relative gene expression of CHK-1, CHK-1-related genes and PARP-1 in KRAS-mutated cell lines CCC16 after treatment with rabusertib. Expression was normalized to untreated CCC16 control cells. Mean ± SD, n=3, p<0.05 (*), p<0.01 (**), p<0.001 (***). B) STRING functional association network between CHK-1 and its regulators and direct/indirect connection with PARP-1.

Figure S1

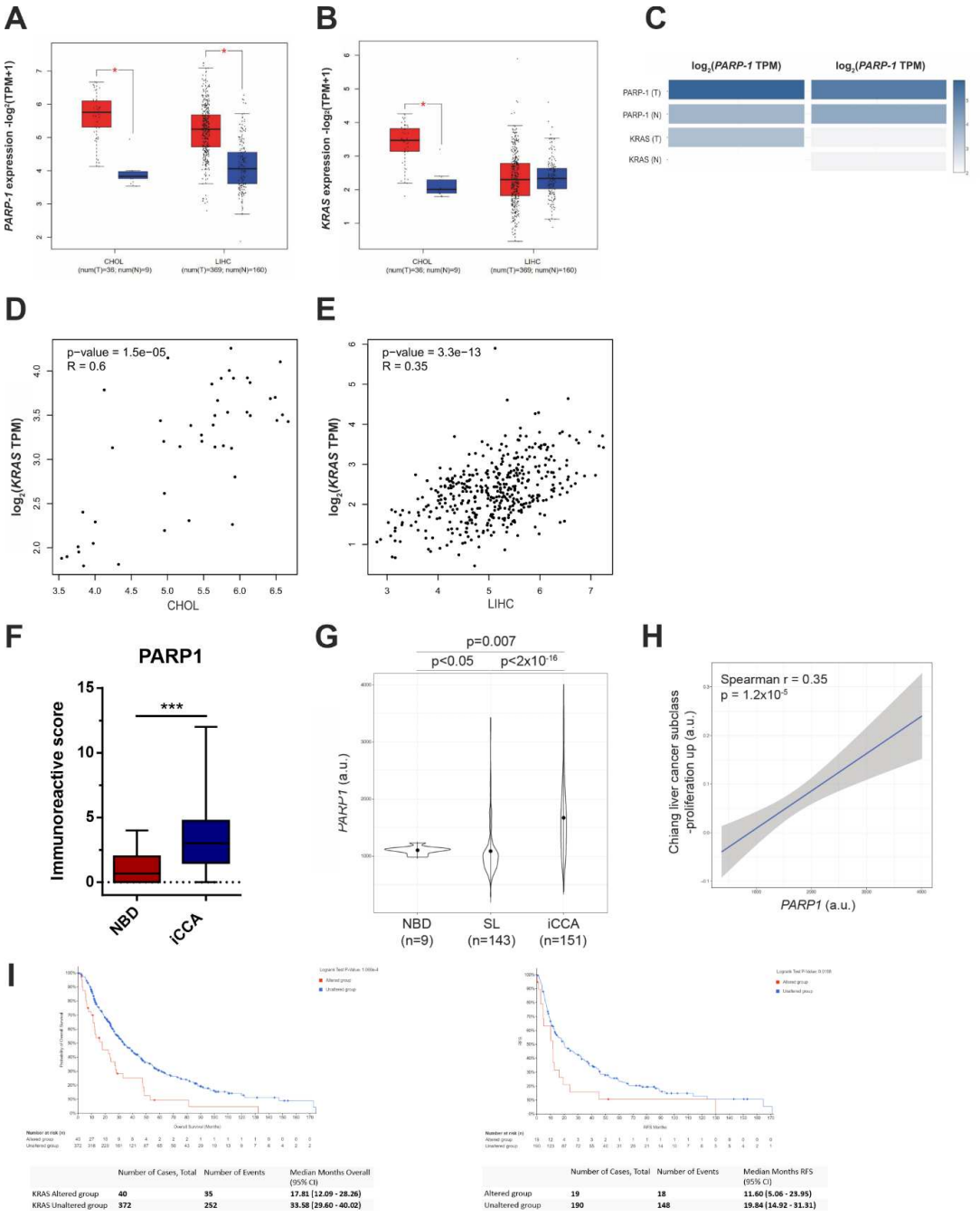
A
PARP-1 expression -log2(TPM+1)
CHOL
(num(T)=36; num(N)=9)
LIHC
(num(T)=369; num(N)=160)
B
KRAS expression -log2(TPM+1)
CHOL
(num(T)=36; num(N)=9)
LIHC
(num(T)=369; num(N)=160)
C
log2(PARP-1 TPM)
log2(PARP-1 TPM)
PARP-1 (T)
PARP-1 (N)
KRAS (T)
KRAS (N)
D
p−value = 1.5e−05
R = 0.6
log2(KRAS TPM)
CHOL
E
p−value = 3.3e−13
R = 0.35
log2(KRAS TPM)
LIHC
F
PARP1
***
Immunoreactive score
NBD
iCCA
G
p=0.007
p<0.05
p<2x10-16
HAIKP1 (a.u.)
NBD
(n=9)
SL
(n=143)
iCCA
(n=151)
H
Spearman r = 0.35
p = 1.2x10-5
Chiang liver cancer subclass
-proliferation up (a.u.)
PARP1 (a.u.)
I
Number of Cases, Total
Number of Events
Median Months Overall (95% CI)
KRAS Altered group 40 35 17.81 [12.09 - 28.26]
KRAS Unaltered group 372 252 33.58 [29.60 - 40.02]
Number of Cases, Total
Number of Events
Median Months RFS (95% CI)
Altered group 19 18 11.60 [5.06 - 23.95]
Unaltered group 190 148 19.84 [14.92 - 31.31]

Figure S2

A

	CCC33	CCC16	WITT	HuH28	HuCCT1	RBE
IC50 [µM]	1175.0 ± 63.88	694.9 ± 148.7	1080.0 ± 129.9	805.3 ± 21.57	387.2 ± 205.5	464.5 ± 80.59

	p-value
CCC33 vs. CCC16	p = 0.0068 (**)
WITT vs. HuCCT1	p = 0.0078 (**)
WITT vs. RBE	p = 0.0026 (**)
WITT vs. HuH28	p = 0.0698 (ns)
HuH28 vs. HuCCT1	p = 0.0725 (ns)
HuH28 vs. RBE	p = 0.0114 (*)
HuCCT1 vs. RBE	p = 0.5769 (ns)

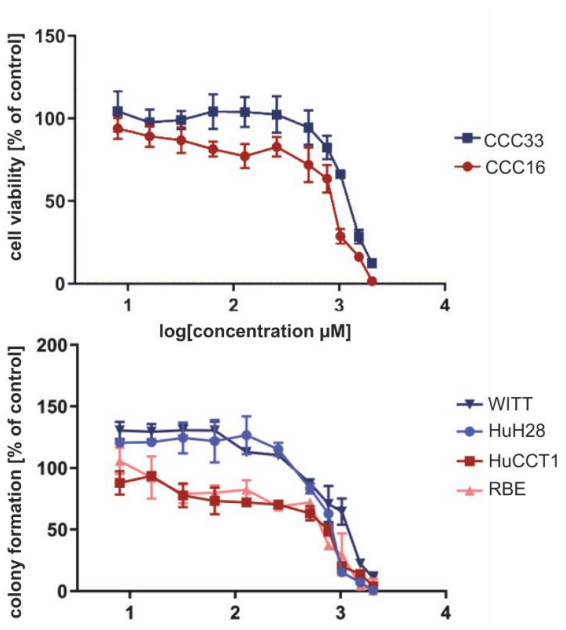

B

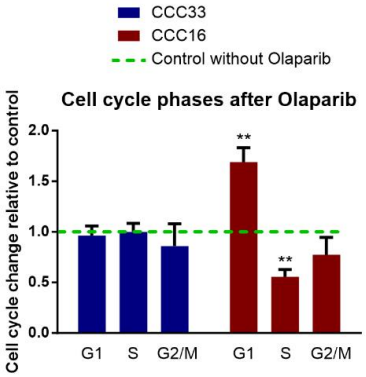

C

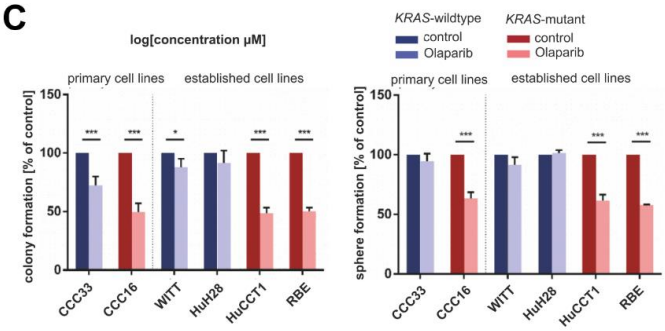

D

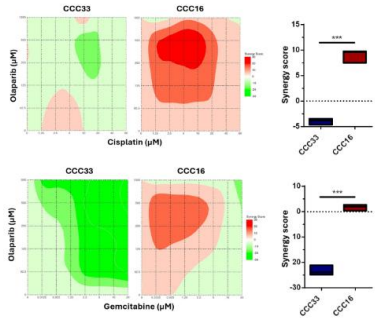

E

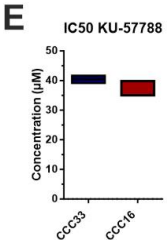

Figure S3

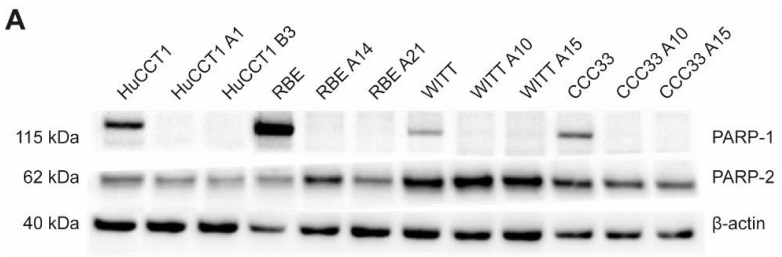
A
HuCCT1
HuCCT1 A1
HuCCT1 B3
RBE
RBE A14
RBE A21
WITT
WITT A10
WITT A15
CCC33
CCC33 A10
CCC33 A15
115 kDa
62 kDa
40 kDa
PARP-1
PARP-2
β-actin

Figure S4

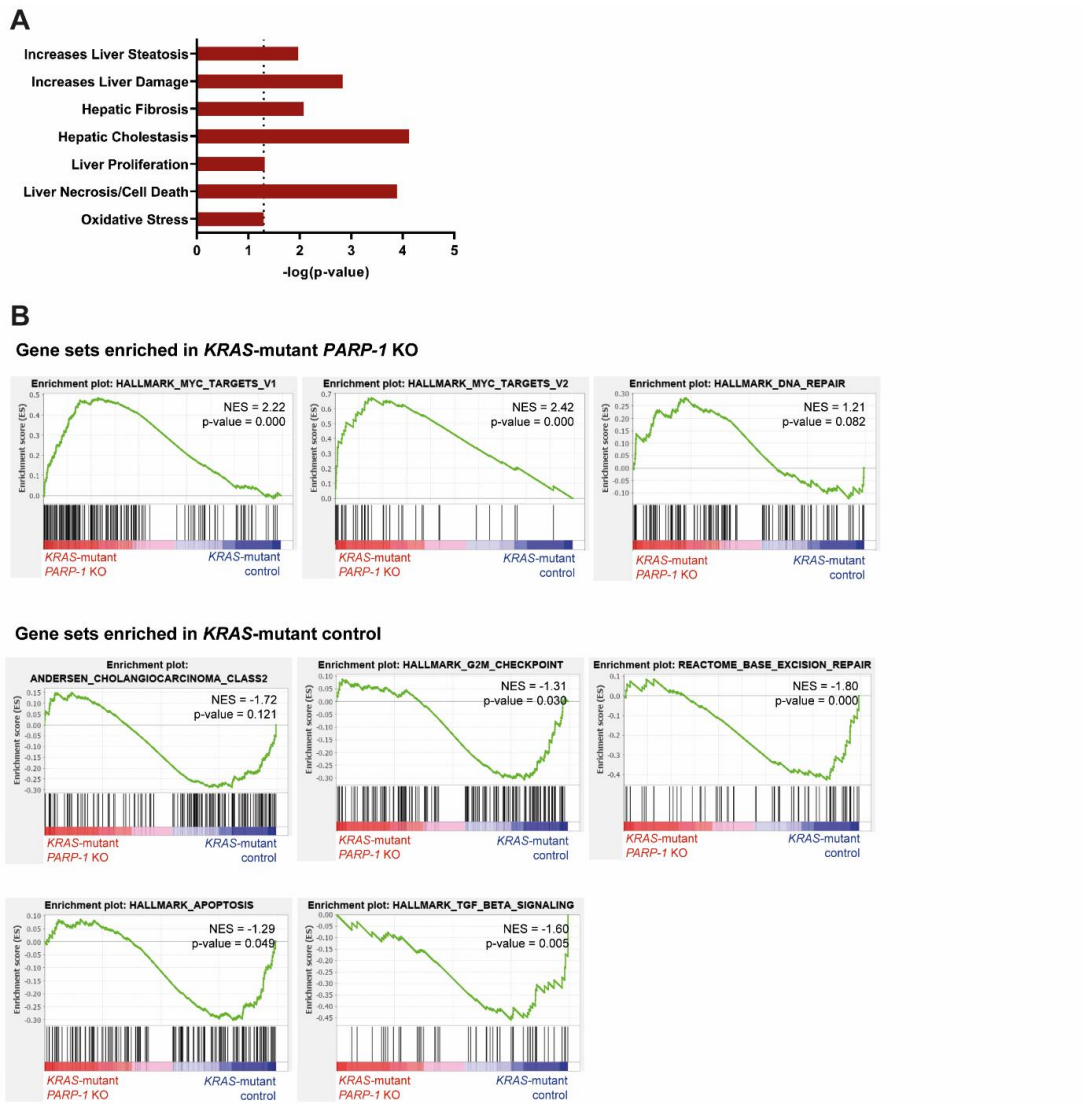
A
Increases Liver Steatosis
Increases Liver Damage
Hepatic Fibrosis
Hepatic Cholestasis
Liver Proliferation
Liver Necrosis/Cell Death
Oxidative Stress
0
1
2
3
4
5
-log(p-value)
B
Gene sets enriched in KRAS-mutant PARP-1 KO
Enrichment plot: HALLMARK_MYC_TARGETS_V1
NES = 2.22
p-value = 0.000
Enrichment plot: HALLMARK_MYC_TARGETS_V2
NES = 2.42
p-value = 0.000
Enrichment plot: HALLMARK_DNA_REPAIR
NES = 1.21
p-value = 0.082
KRAS-mutant PARP-1 KO
KRAS-mutant control
Gene sets enriched in KRAS-mutant control
Enrichment plot: ANDERSEN_CHOLANGIOCARCINOMA_CLASS2
NES = -1.72
p-value = 0.121
Enrichment plot: HALLMARK_G2M_CHECKPOINT
NES = -1.31
p-value = 0.030
Enrichment plot: REACTOME_BASE_EXCISION_REPAIR
NES = -1.80
p-value = 0.000
Enrichment plot: HALLMARK_APOPTOSIS
NES = -1.29
p-value = 0.049
Enrichment plot: HALLMARK_TGF_BETA_SIGNALING
NES = -1.60
p-value = 0.005
Enrichment score (ES)

Figure S5

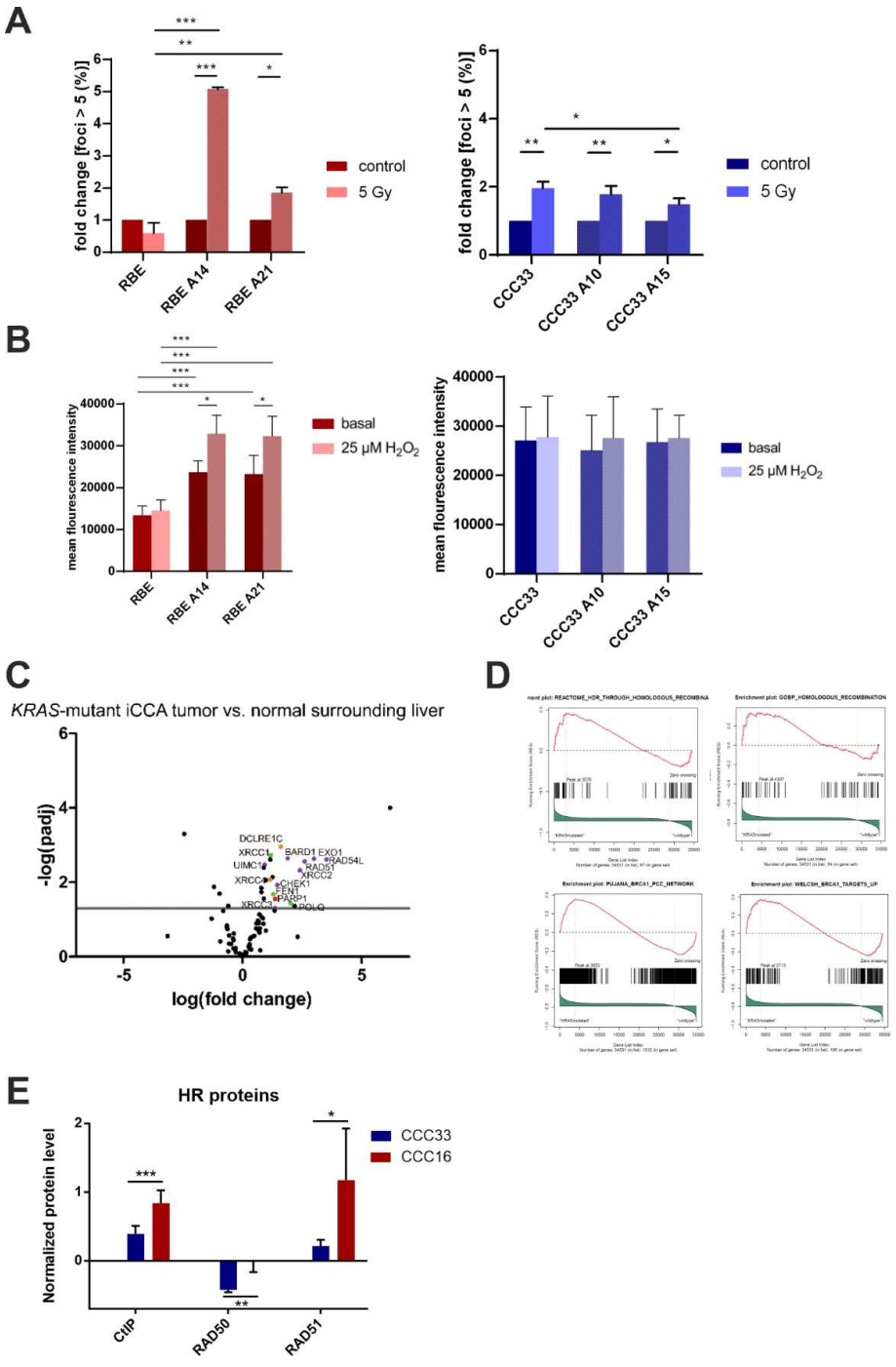
A
fold change [foci > 5 (%)]
control
5 Gy
RBE
RBE A14
RBE A21
CCC33
CCC33 A10
CCC33 A15
B
mean flourescence intensity
basal
25 μM H2O2
C
KRAS-mutant iCCA tumor vs. normal surrounding liver
-log(padj)
log(fold change)
DCLRE1C
XRCC1
BARD1
EXO1
RAD54L
UIMC1
RAD51
XRCC2
XRCC4
CHEK1
FEN1
PARP1
POLQ
D
E
HR proteins
Normalized protein level
CCC33
CCC16
ChIP
RAD50
RAD51

Figure S6

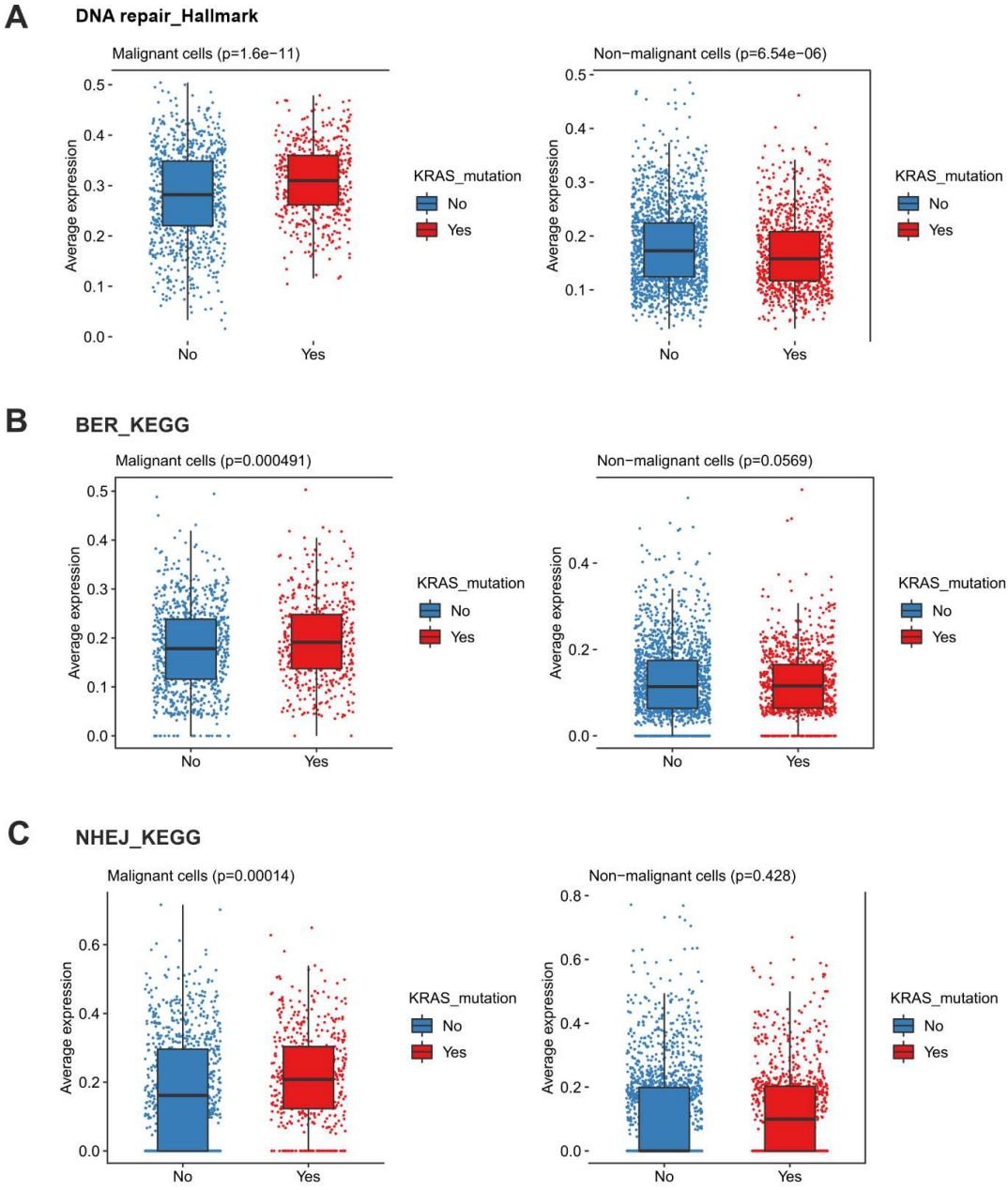
A
DNA repair_Hallmark
Malignant cells (p=1.6e−11)
Non−malignant cells (p=6.54e−06)
Average expression
KRAS_mutation
No
Yes
B
BER_KEGG
Malignant cells (p=0.000491)
Non−malignant cells (p=0.0569)
C
NHEJ_KEGG
Malignant cells (p=0.00014)
Non−malignant cells (p=0.428)

Figure S7

A

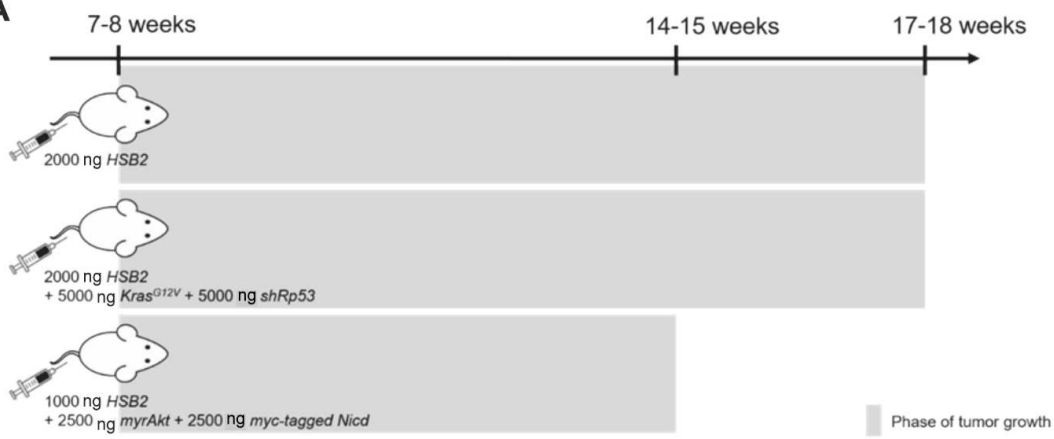

B

Injection (plasmid)	genotype	ID	gender	body weight [g]	liver weight [g]
Empty vector	*PARP-1 +/+*	MAR-F947	male	32.5	1.1
		MAR-F990		32.1	1.2
		MAR-G049		32.6	1.9
		MAR-G511		31.1	1.4
		MAR-G513		32.6	1.4
	PARP-1 -/-	MAR-F997	male	36.3	1.6
		MAR-G003		26.9	1.3
		MAR-G048		35.3	1.8
		MAR-G060		31.3	1.7
		MAR-G507		32.3	1.3
Kras/Tp53	*PARP-1 +/+*	MAR-G032	male	26.5	2.7
		MAR-G149		26.0	2.4
		MAR-G419		30.1	2.6
		MAR-G457*		27.4	2.7
		MAR-G500		28.8	3.4
	PARP-1 -/-	MAR-G100	male	27.9	6.9
		MAR-G101		29.8	6.2
		MAR-G180		30.3	5.9
		MAR-G336		30.3	6.2
		MAR-G458		29.0	5.5
		MAR-G459		30.7	5.9
Akt/Nicd	*PARP-1 +/+*	MAR-F944	male	36.7	8.7
		MAR-F991		30.0	6.0
		MAR-G012		31.7	6.7
		MAR-G080		34.0	5.1
		MAR-G133		30.5	5.1
	PARP-1 -/-	MAR-G036	male	32.2	6.0
		MAR-G063		29.1	5.1
		MAR-G066		31.9	6.1
		MAR-G139		29.4	4.7
		MAR-G140		27.2	4.1

Figure S8

A

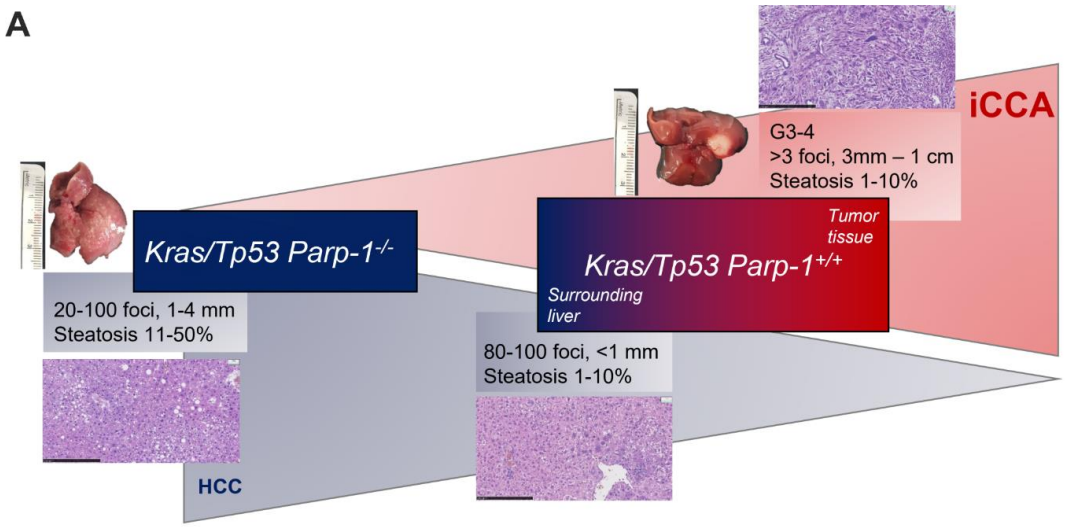

B

plasmid	N	genotype	tissue	classification	grading	foci	size	hematogenous spread
Empty vector (HSB2)	5	*PARP-1 +/+*	**normal liver**	No tumor	-	-	-	-
	5	*PARP-1 -/-*	**normal liver**	No tumor	-	-	-	-
Kras/Tp53	5	*PARP-1 +/+*	**tumor**	4x iCCA, 1x iCCA-HCC	G3-4	>3	3 mm – 1 cm	-
			dysplastic foci in normal liver	5x dysplastic foci	n.A.	80-100	<1 mm	V1
	6	*PARP-1 -/-*	**dysplastic foci in normal liver**	6x dysplastic foci, 1x HCC	n.A.	20-100	1-4 mm	V1
Akt/Nicd	5	*PARP-1 +/+*	**tumor in normal liver**	Multiple iCCA	G1-2	~100	1-4 mm	-
	5	*PARP-1 -/-*		Multiple iCCA	G1-2	~100	1-4 mm	-

Figure S9

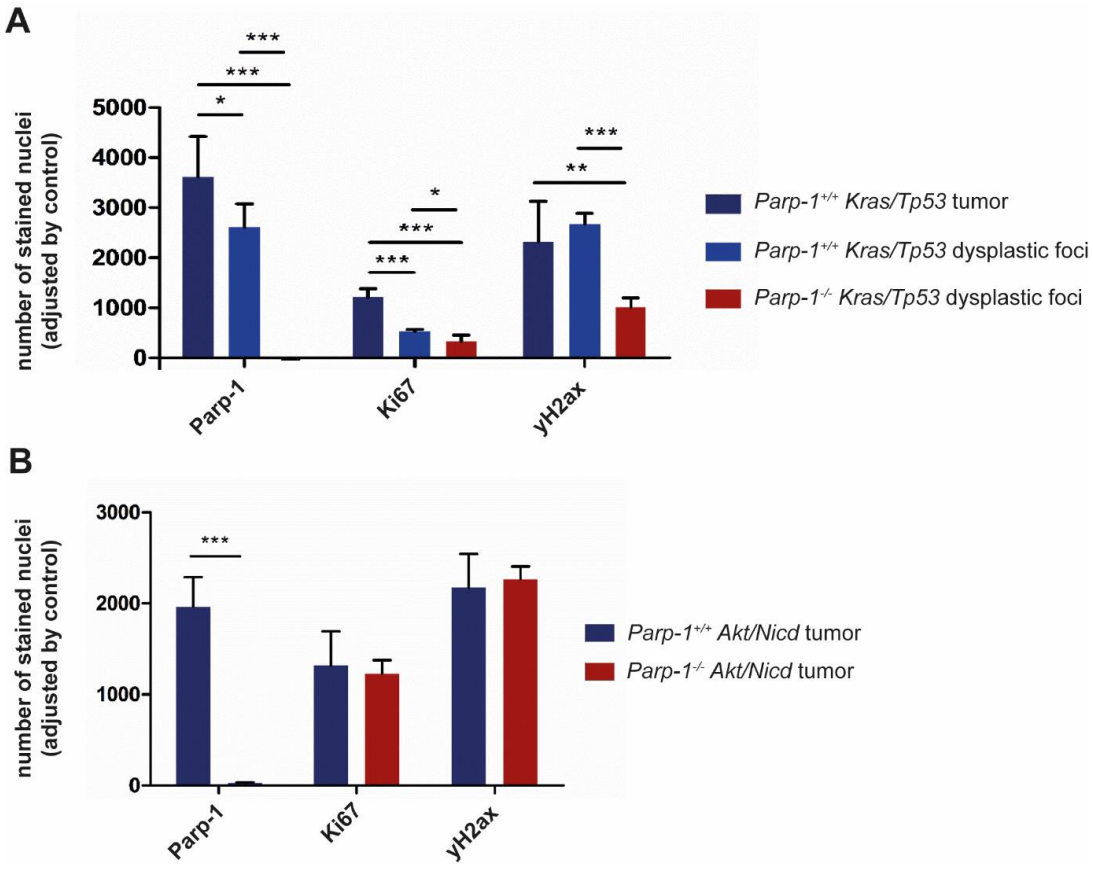
A
number of stained nuclei (adjusted by control)
5000
4000
3000
2000
1000
0
***
***
*
***
***
*
***
**
Parp-1
Ki67
γH2ax
Parp-1+/+ Kras/Tp53 tumor
Parp-1+/+ Kras/Tp53 dysplastic foci
Parp-1-/- Kras/Tp53 dysplastic foci
B
number of stained nuclei (adjusted by control)
3000
2000
1000
0
***
Parp-1
Ki67
γH2ax
Parp-1+/+ Akt/Nicd tumor
Parp-1-/- Akt/Nicd tumor

Figure S10

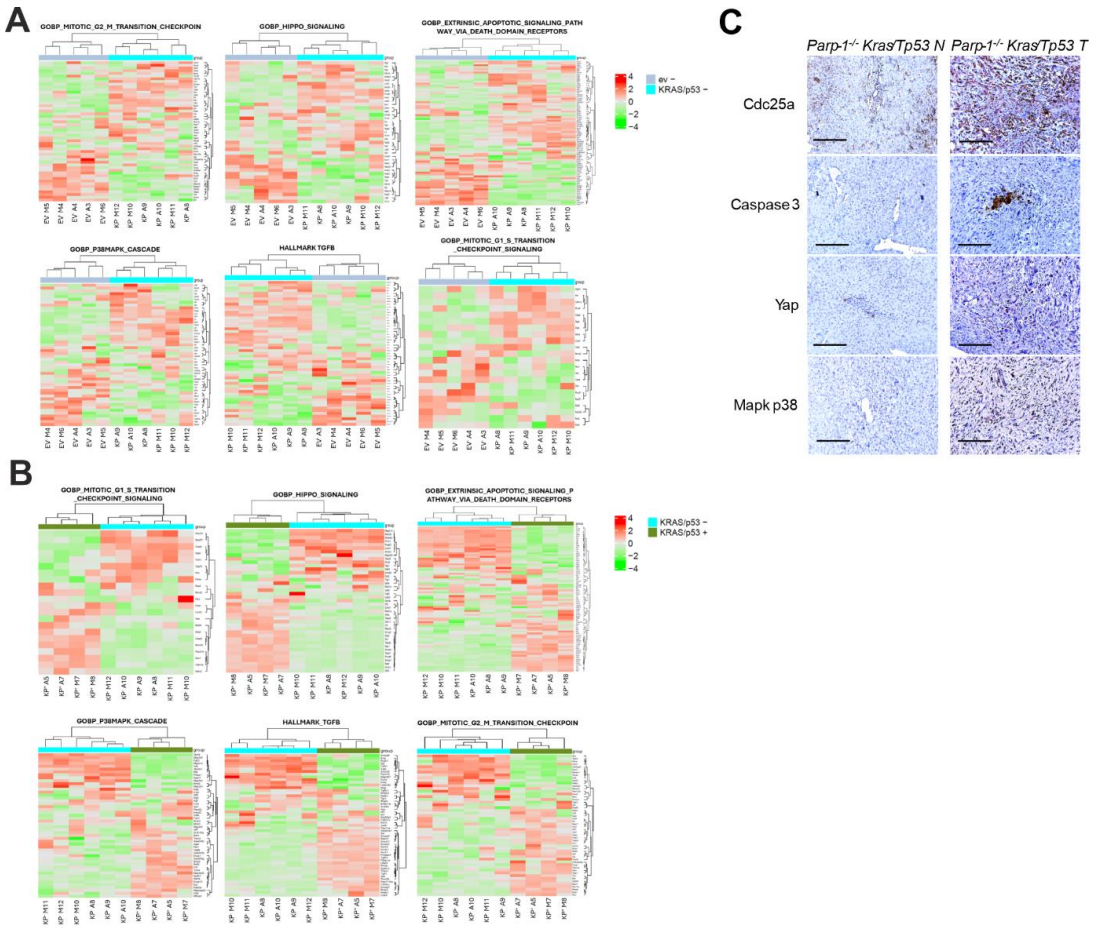
A
GOBP_MITOTIC_G2_M_TRANSITION_CHECKPOIN
GOBP_HIPPO_SIGNALING
GOBP_EXTRINSIC_APOPTOTIC_SIGNALING_PATH WAY_VIA_DEATH_DOMAIN_RECEPTORS
GOBP_P38MAPK_CASCADE
HALLMARK_TGFB
GOBP_MITOTIC_G1_S_TRANSITION _CHECKPOINT_SIGNALING
4
2
0
−2
−4
ev −
KRAS/p53 −
B
GOBP_MITOTIC_G1_S_TRANSITION _CHECKPOINT_SIGNALING
GOBP_HIPPO_SIGNALING
GOBP_EXTRINSIC_APOPTOTIC_SIGNALING_P ATHWAY_VIA_DEATH_DOMAIN_RECEPTORS
GOBP_P38MAPK_CASCADE
HALLMARK_TGFB
GOBP_MITOTIC_G2_M_TRANSITION_CHECKPOIN
4
2
0
−2
−4
KRAS/p53 −
KRAS/p53 +
C
Parp-1-/- KrasTp53 N
Parp-1-/- KrasTp53 T
Cdc25a
Caspase 3
Yap
Mapk p38

Figure S11

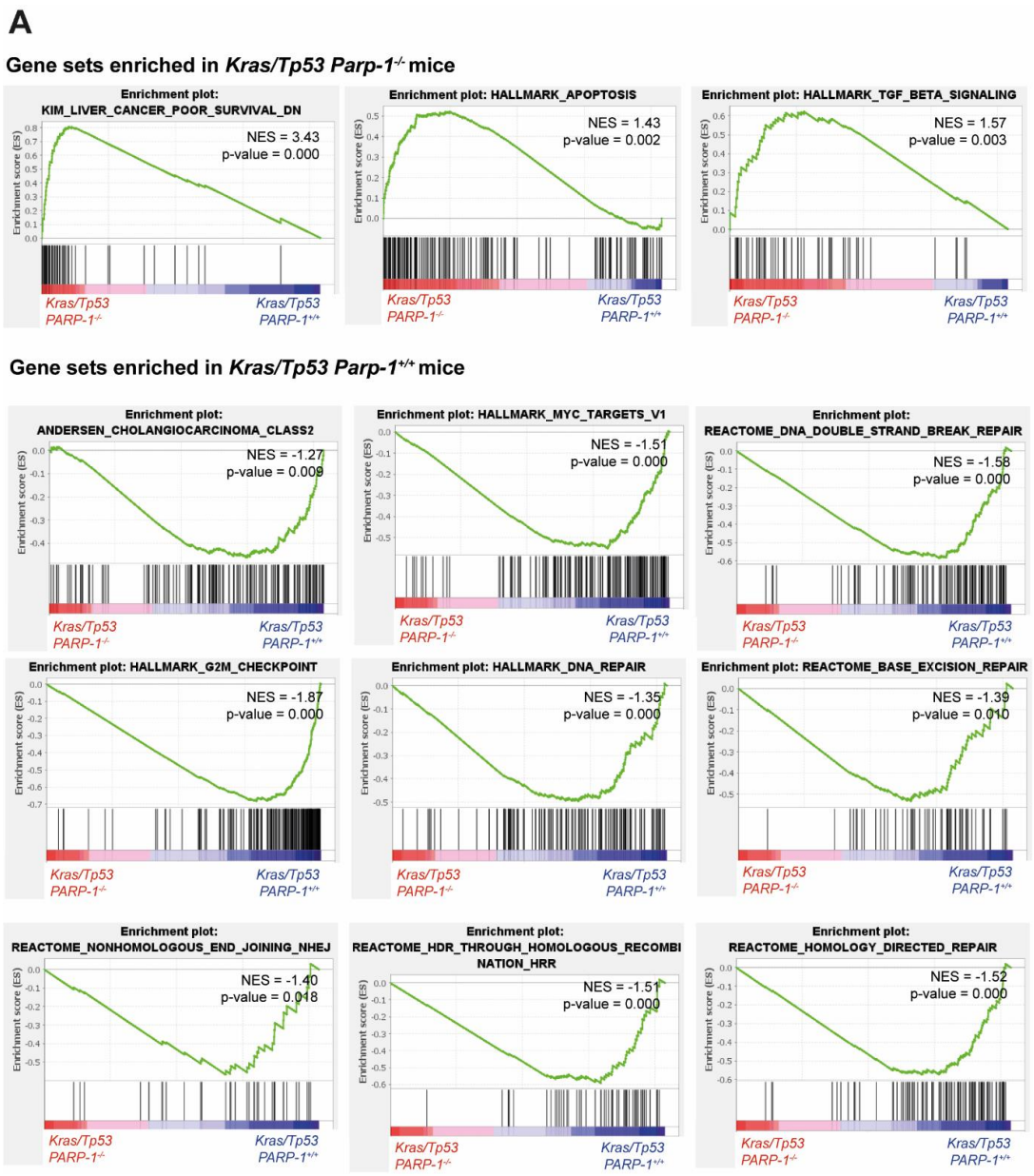
A
Gene sets enriched in Kras/Tp53 Parp-1-/- mice
Enrichment plot: KIM_LIVER_CANCER_POOR_SURVIVAL_DN
NES = 3.43
p-value = 0.000
Enrichment plot: HALLMARK_APOPTOSIS
NES = 1.43
p-value = 0.002
Enrichment plot: HALLMARK_TGF_BETA_SIGNALING
NES = 1.57
p-value = 0.003
Gene sets enriched in Kras/Tp53 Parp-1+/+ mice
Enrichment plot: ANDERSEN_CHOLANGIOCARCINOMA_CLASS2
NES = -1.27
p-value = 0.009
Enrichment plot: HALLMARK_MYC_TARGETS_V1
NES = -1.51
p-value = 0.000
Enrichment plot: REACTOME_DNA_DOUBLE_STRAND_BREAK_REPAIR
NES = -1.58
p-value = 0.000
Enrichment plot: HALLMARK_G2M_CHECKPOINT
NES = -1.87
p-value = 0.000
Enrichment plot: HALLMARK_DNA_REPAIR
NES = -1.35
p-value = 0.000
Enrichment plot: REACTOME_BASE_EXCISION_REPAIR
NES = -1.39
p-value = 0.010
Enrichment plot: REACTOME_NONHOMOLOGOUS_END_JOINING_NHEJ
NES = -1.40
p-value = 0.018
Enrichment plot: REACTOME_HDR_THROUGH_HOMOLOGOUS_RECOMBINATION_HRR
NES = -1.51
p-value = 0.000
Enrichment plot: REACTOME_HOMOLOGY_DIRECTED_REPAIR
NES = -1.52
p-value = 0.000
Enrichment score (ES)
Kras/Tp53 PARP-1-/-
Kras/Tp53 PARP-1+/+

Figure S12

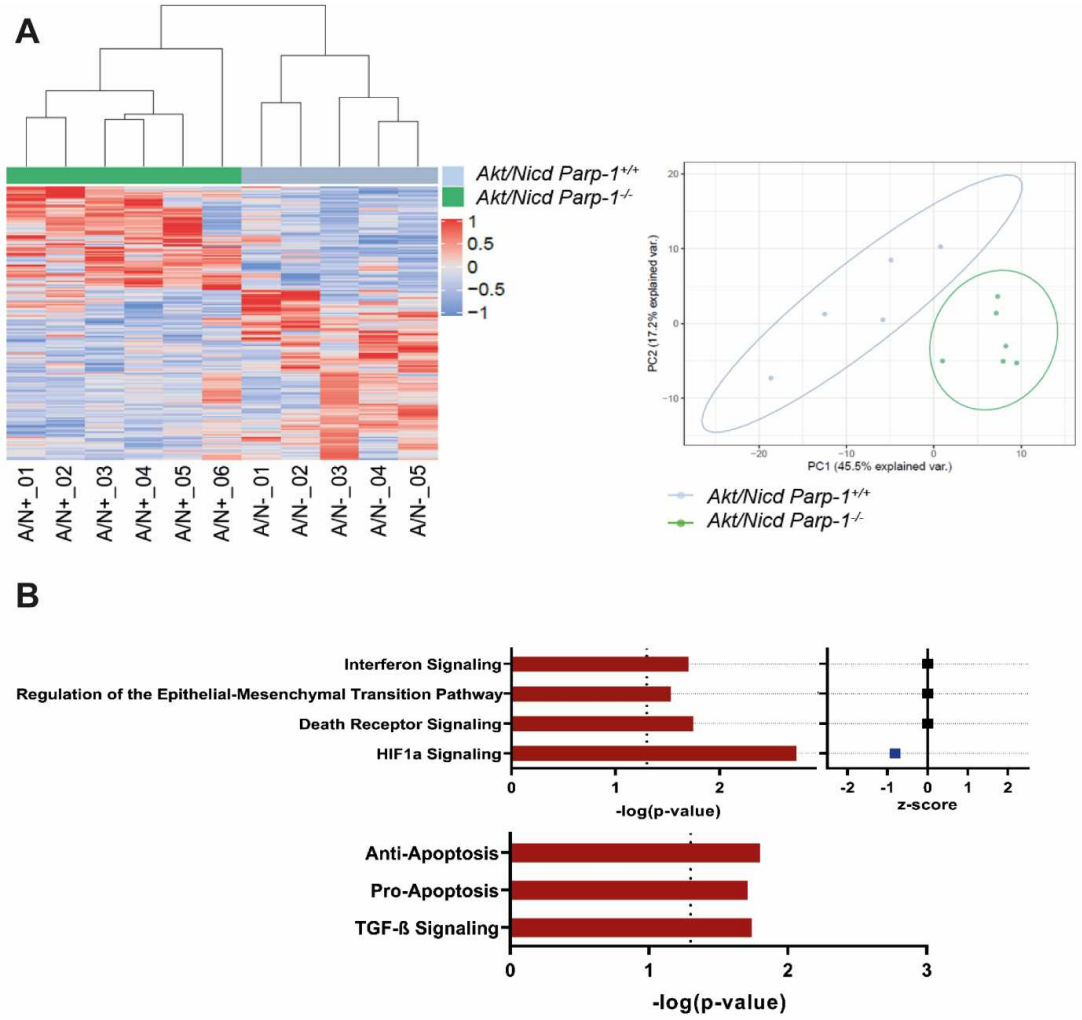
A
Akt/Nicd Parp-1+/+
Akt/Nicd Parp-1-/-
1
0.5
0
−0.5
−1
A/N+_01
A/N+_02
A/N+_03
A/N+_04
A/N+_05
A/N+_06
A/N-_01
A/N-_02
A/N-_03
A/N-_04
A/N-_05
PC2 (17.2% explained var.)
PC1 (45.5% explained var.)
Akt/Nicd Parp-1+/+
Akt/Nicd Parp-1-/-
B
Interferon Signaling
Regulation of the Epithelial-Mesenchymal Transition Pathway
Death Receptor Signaling
HIF1a Signaling
-log(p-value)
z-score
Anti-Apoptosis
Pro-Apoptosis
TGF-ß Signaling
-log(p-value)

Figure S13

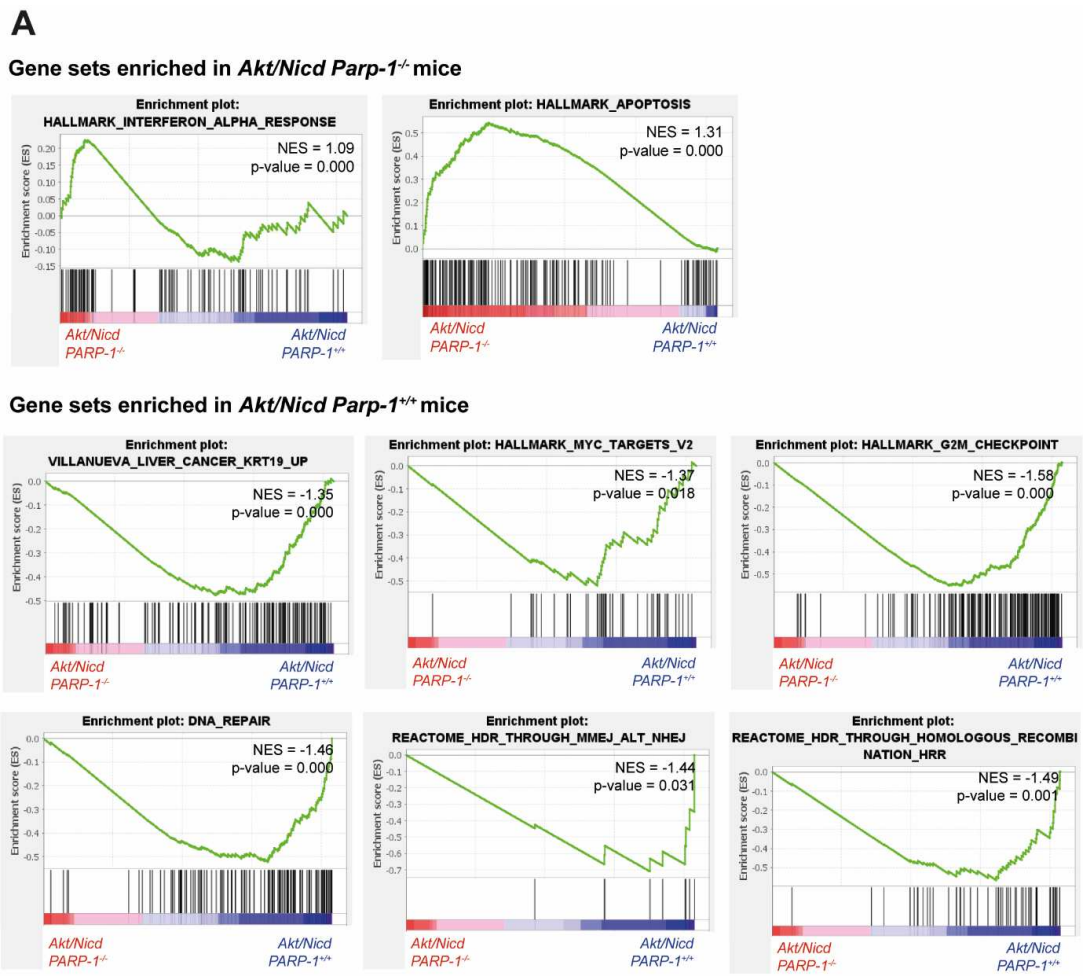
A
Gene sets enriched in Akt/Nicd Parp-1-/- mice
Enrichment plot: HALLMARK_INTERFERON_ALPHA_RESPONSE
NES = 1.09
p-value = 0.000
Enrichment plot: HALLMARK_APOPTOSIS
NES = 1.31
p-value = 0.000
Gene sets enriched in Akt/Nicd Parp-1+/+ mice
Enrichment plot: VILLANUEVA_LIVER_CANCER_KRT19_UP
NES = -1.35
p-value = 0.000
Enrichment plot: HALLMARK_MYC_TARGETS_V2
NES = -1.37
p-value = 0.018
Enrichment plot: HALLMARK_G2M_CHECKPOINT
NES = -1.58
p-value = 0.000
Enrichment plot: DNA_REPAIR
NES = -1.46
p-value = 0.000
Enrichment plot: REACTOME_HDR_THROUGH_MMEJ_ALT_NHEJ
NES = -1.44
p-value = 0.031
Enrichment plot: REACTOME_HDR_THROUGH_HOMOLOGOUS_RECOMBINATION_HRR
NES = -1.49
p-value = 0.001
Enrichment score (ES)
Akt/Nicd PARP-1-/-
Akt/Nicd PARP-1+/+

Figure S14

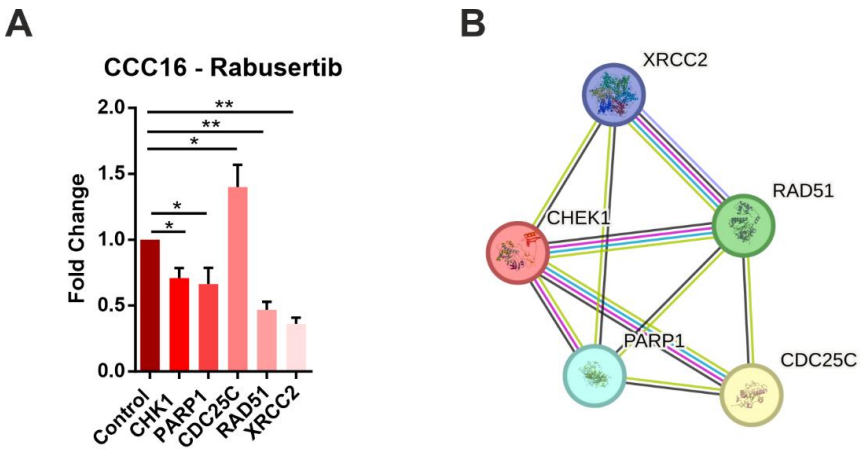
A
CCC16 - Rabusertib
Fold Change
2.0
1.5
1.0
0.5
0.0
**
**
*
*
*
Control
CHK1
PARP1
CDC25C
RAD51
XRCC2
B
XRCC2
RAD51
CHEK1
PARP1
CDC25C

References:

1 Castven D, Becker D, Czauderna C, *et al.* Application of patient-derived liver cancer cells for phenotypic characterization and therapeutic target identification. *Int J Cancer*. 2019;144:2782–94.
2 Andersen JB, Spee B, Blechacz BR, *et al.* Genomic and genetic characterization of cholangiocarcinoma identifies therapeutic targets for tyrosine kinase inhibitors. *Gastroenterology*. 2012;142:1021-1031.e15.
3 Castven D, Fischer M, Becker D, *et al.* Adverse genomic alterations and stemness features are induced by field cancerization in the microenvironment of hepatocellular carcinomas. *Oncotarget*. 2017;8:48688–700.
4 Massa A, Varamo C, Vita F, *et al.* Evolution of the Experimental Models of Cholangiocarcinoma. *Cancers*. 2020;12:2308.
5 Gu Z, Eils R, Schlesner M. Complex heatmaps reveal patterns and correlations in multidimensional genomic data. *Bioinforma Oxf Engl*. 2016;32:2847–9.
6 Krämer A, Green J, Pollard J, *et al.* Causal analysis approaches in Ingenuity Pathway Analysis. *Bioinforma Oxf Engl*. 2014;30:523–30.
7 Subramanian A, Tamayo P, Mootha VK, *et al.* Gene set enrichment analysis: a knowledge-based approach for interpreting genome-wide expression profiles. *Proc Natl Acad Sci U S A*. 2005;102:15545–50.
8 Tang Z, Kang B, Li C, *et al.* GEPIA2: an enhanced web server for large-scale expression profiling and interactive analysis. *Nucleic Acids Res*. 2019;47:W556–60.
9 O'Dell MR, Huang JL, Whitney-Miller CL, *et al.* Kras(G12D) and p53 mutation cause primary intrahepatic cholangiocarcinoma. *Cancer Res*. 2012;72:1557–67.
10 de Murcia JM, Niedergang C, Trucco C, *et al.* Requirement of poly(ADP-ribose) polymerase in recovery from DNA damage in mice and in cells. *Proc Natl Acad Sci U S A*. 1997;94:7303–7.
11 Matter MS, Marquardt JU, Andersen JB, *et al.* Oncogenic driver genes and the inflammatory microenvironment dictate liver tumor phenotype. *Hepatol Baltim Md*. 2016;63:1888–99.
12 Chen X, Calvisi DF. Hydrodynamic transfection for generation of novel mouse models for liver cancer research. *Am J Pathol*. 2014;184:912–23.
13 Saborowski A, Saborowski M, Davare MA, *et al.* Mouse model of intrahepatic cholangiocarcinoma validates FIG-ROS as a potent fusion oncogene and therapeutic target. *Proc Natl Acad Sci U S A*. 2013;110:19513–8.
14 Remmele W, Stegner HE. [Recommendation for uniform definition of an immunoreactive score (IRS) for immunohistochemical estrogen receptor detection (ER-ICA) in breast cancer tissue]. *Pathol*. 1987;8:138–40.
15 Szklarczyk D, Kirsch R, Koutrouli M, *et al.* The STRING database in 2023: protein-protein association networks and functional enrichment analyses for any sequenced genome of interest. *Nucleic Acids Res*. 2023;51:D638–46.